Geophysical Research Letters

RESEARCH LETTER
10.1029/2024GL112305

Macau Scientific Satellite-1 Initial Magnetic Field Model

Yi Jiang[1,2], Christopher C. Finlay[3], Nils Olsen[3], Lars Tøffner-Clausen[3], Qing Yan[1,2,4], and Keke Zhang[1,2]

[1]Macau Institute of Space Technology and Application, Macau University of Science and Technology, Macau, China, [2]Zhuhai MUST Science and Technology Research Institute, Zhuhai, China, [3]Division of Geomagnetism and Geospace, DTU Space, National Space Institute, Technical University of Denmark, Kgs. Lyngby, Denmark, [4]State Key Laboratory of Lunar and Planetary Sciences, Macau University of Science and Technology, Macau, China

Key Points:

- Macau Scientific Satellite-1 provides the first vector magnetic field measurements with absolute accuracy from a low inclination orbit
- Geomagnetic field models constructed using vector data only from MSS-1 are suitable for scientific studies of core and lithospheric fields
- By covering all local times within 2 months, MSS-1 provides a new class of observational constraints on rapid geomagnetic field variations

Supporting Information:

Supporting Information may be found in the online version of this article.

Correspondence to:

Y. Jiang,
yjiang@must.edu.mo

Citation:

Jiang, Y., Finlay, C. C., Olsen, N., Tøffner-Clausen, L., Yan, Q., & Zhang, K. (2024). Macau Scientific Satellite-1 initial magnetic field model. *Geophysical Research Letters*, *51*, e2024GL112305. https://doi.org/10.1029/2024GL112305

Received 4 SEP 2024
Accepted 6 NOV 2024

Abstract Eight months of vector magnetic field measurements from the Macau Scientific Satellite-1 (MSS-1), supplemented by higher latitude field intensity measurements from the *Swarm* satellites, are used to derive an MSS-1 Initial Field Model (MIFM). Robust root-mean-square misfits between MIFM and the three components of the MSS-1 vector field data are found to be below 3.3 nT. MIFM agrees well with the CHAOS-7 field model and we find even better agreement with an identically parameterized model derived only from *Swarm* data. MSS-1 and *Swarm* vector data can moreover be fit simultaneously with only a small increase in misfit (by less than 0.2 nT). We show that both lithospheric anomalies and core surface field changes can be studied using MSS-1 data. With its fast coverage of local times MSS-1 is a valuable addition to the global geomagnetic observing system.

Plain Language Summary Earth's magnetic field is an essential part of our planetary environment. The global state of the field and its time variations are today carefully monitored from space by satellites. However rather few satellites provide measurements with the accuracy needed for detailed scientific studies and for the construction of geomagnetic reference models used for navigation. We show that vector magnetic field measurements from the Macau Scientific Satellite 1 (MSS-1), launched in May 2023, are suitable for building high quality reference models of Earth's magnetic field. We show that time changes of field at the core-mantle boundary and field anomalies related to lithospheric magnetization can be mapped using an initial 8 months of MSS-1 data. Thanks to its low inclination orbit, MSS-1 covers all local times, for latitudes up to ±41°, within 2 months. This complements the coverage of existing polar-orbiting satellites and provides new opportunities to study rapid geomagnetic field changes.

1. Introduction

The global state of the Earth's magnetic field is today carefully monitored by low-Earth-orbit magnetic survey satellites. These collect observations of Earth's vector magnetic field by combining measurements from high precision three-axis fluxgate magnetometers (calibrated by independent absolute measurements of the field intensity) with attitude information from co-located star trackers. ESA's *Swarm* satellite trio (Friis-Christensen et al., 2006) has since 2013 been the primary source of such observations. One limitation of the data provided by *Swarm* is the restricted local-time coverage, a consequence of the high inclination polar orbits of all three satellites, and because two of the three satellites fly close together as a pair. Each *Swarm* satellite covers all local times, measured by the equatorial crossing of the ascending node of the orbit, in 267 days (8.8 months). This means that between 4.4 and 2.2 months are needed to have a complete picture of local time-dependent fields, depending on the configuration of the satellite trio. Lack of knowledge of local-time dependent fields, for instance ionospheric fields, results in a limited temporal resolution of the core-generated field.

The global observing system monitoring Earth's magnetic field has been significantly enhanced with the launch of the Macau Scientific Satellite-1 mission (K. Zhang, 2023) by the China National Space Administration and Macau Government on 21 May 2023. The MSS-1 mission involves two spacecraft flying in near-circular orbits with inclination 41° at 430 km altitude as of June 2024. The equatorial crossing of the ascending node covers all local times in just 53 days (1.8 months). Considering both ascending and descending part of the orbits this means that all local times are covered within 27 days (0.9 months) although not evenly at all latitudes. All local times are covered at all latitudes by MSS-1 within 53 days. One of the spacecraft (MSS-1A) carries a magnetometry package designed to provide high-precision magnetic data with excellent quality and absolute accuracy. The

second satellite (MSS-1B) focuses on energetic electron flux and solar X-ray detection and does not perform magnetic field measurements (Jiang et al., 2023; Shi et al., 2023). The availability of high quality absolute measurements of the vector magnetic field covering local times faster than previous magnetic survey satellites opens new possibilities for exploring and monitoring rapid changes in Earth's magnetic field.

The magnetometry package on MSS-1A is mounted on a 430 cm long boom and includes a Coupled Dark State Magnetometer (CDSM) providing absolute measurements of Earth's magnetic field intensity, two vector magnetometers and a non-magnetic three-head Micro Advanced Stellar Compass (ASC) providing attitude information (Jørgensen et al., 2003). The ASC and one of the vector magnetometers, the Vector Fluxgate Magnetometer (Brauer et al., 2001; Merayo et al., 2000) denoted VFM, are mounted close together on an optical bench on the boom (H. Zhang et al., 2023). The other vector fluxgate magnetometer (denoted FGM), is 80 cm away from the optical bench. In this study we use only data from the VFM and not from the FGM. Position and time information are provided by a GNSS receiver. MSS-1 data and further information are available at https://mss.must.edu.mo/index.html.

In this letter, we report on the quality of the MSS-1 vector magnetic field data and its suitability for global field modeling by presenting an initial field model (the MIFM model) that uses an initial 8 months of data from MSS-1A. At latitudes poleward of ±40° where, as a result of its low inclination orbit, MSS-1 data are not available we instead use field intensity measurements collected by the *Swarm* A and B satellites. The parameterization of MIFM is on purpose rather simple, since our focus here is to illustrate the quality of MSS-1 data. For the internal field we allow for linear secular variation over the considered 8 months. For the external field we adopt the same model parameterization as used in the CHAOS field model series (Olsen et al., 2006, 2014). We also report results from test models parameterized in the same way but including both MSS-1 and *Swarm* vector data at non-polar latitudes (Model 1), and respectively only using *Swarm* (vector and scalar) data (Model_sw). We find excellent consistency of MSS-1 and *Swarm* data and demonstrate that MSS-1 vector data are well suited for scientific studies of the core and lithospheric fields. The purpose of this letter is to present, using rather simple field models, the quality of the vector magnetic field data provided by MSS-1 by comparing it with data from the *Swarm* satellites. Taking full advantage of the rapid local-time coverage provided by MSS-1 will require more advanced treatments of magnetospheric and ionospheric fields which will be the subject of future studies.

2. Data Selection

To construct MIFM we use nearly 8 months (2 November 2023–30 June 2024) of magnetic observations collected by MSS-1A, supplemented by observations from the *Swarm* mission.

Calibration studies carried out during commissioning phase of the MSS-1 mission have demonstrated the high quality and absolute accuracy of the vector magnetic field observations collected by MSS-1. During the in-flight calibration of the magnetometry package a Huber weighted rms misfit of less than 260 pT, between the CDSM absolute scalar magnetometer and the magnetic field intensity from the vector magnetometer (VFM), was found. This indicates MSS-1 vector magnetic field measurements are of comparable quality to those of the *Swarm* mission. Here, we use 1 Hz MSS-1 vector field observations, publicly released data version TEST 04, down-sampled to 30 s.

Regarding data from the *Swarm* mission, we use the MAGX_LR_1B, 1 Hz calibrated data product, baseline 06, from the *Swarm-A* and *Swarm-B* satellites, also with 30 s sampling, taken from the same 8 month period.

We use the following criteria to select data suitable for field modeling from both the MSS-1 and the *Swarm* satellites. To focus on the internal field and avoid strong geomagnetic disturbances due to external sources we use data only from geomagnetically quiet conditions such that (a) the geomagnetic activity index $Kp \leq 2o$ and (b) the strength of the magnetic signature of the magnetospheric ring current, described using the RC index (Olsen et al., 2014), changes by at most 2 nT/hr. To minimize the signatures of ionospheric current systems we use (c) non-polar data only from dark regions (Sun at least 10° below horizon) and (d) polar data only for local times after 18:00 and before 6:00. To reduce the impact of strong and highly dynamic field aligned currents in the polar region we use (e) vector data only at non-polar latitudes. We define the polar region to be above ±60° quasi-dipole (QD) latitude (Richmond, 1995).

In building MIFM, we used vector field data only from MSS-1 (103,944 vector triples) and scalar data only from *Swarm* (82,560 intensity measurements from *Swarm* A and 85,427 from *Swarm* B) at geographic latitudes poleward of ±40° where MSS-1 data are not available due to its orbit. To test the compatibility of *Swarm* and MSS-1 vector data we constructed two additional models using the same model parameterization but based on different data combinations: Model 1 uses both MSS-1 and *Swarm* A and B vector data below ±60° QD latitude and *Swarm* A and B scalar data at higher QD latitudes. Model_sw uses data only from *Swarm* A and B, vector data below ±60° QD latitude and scalar data at higher QD latitudes.

Figure 1 illustrates the distribution of MSS-1 and *Swarm* data used to build MIFM as a function of time and latitude. Variations in the amount of data with time are a result of the selection criteria discussed above. Note that more MSS-1 data are available close to latitudes ±40° due to its orbital configuration.

3. Model Parameterization and Estimation

MIFM was constructed as follows. The vector magnetic field $\mathbf{B} = -\nabla V$ is represented as the gradient of a scalar potential $V = V^{int} + V^{ext}$, where V^{int} represents internal sources and V^{ext} external sources. For the internal field, we expand V^{int} in spherical harmonics such that

$$V^{int} = a \sum_{n=1}^{N_{\max}} \sum_{m=0}^{n} \left(\frac{a}{r}\right)^{n+1} \left[g_n^m(t)\cos m\phi + h_n^m(t)\sin m\phi\right] P_n^m(\cos\theta) \quad (1)$$

where $a = 6371.2$ km is the Earth's spherical reference radius. (r, θ, ϕ) are spherical radial distance, co-latitude and longitude in the geographical coordinate system. $P_n^m(\cos\theta)$ are Schmidt semi-normalized associated Legendre functions of degree n and order m (Winch et al., 2005).

The model coefficients $\{g_n^m(t), h_n^m(t)\}$, also known as Gauss coefficients, thus specify the internal field as a function of time. We allow a linear time dependence of the Gauss coefficients over our model timespan

$$g_n^m(t) = g_n^m(t_0) + \dot{g}_n^m(t_0)\cdot(t - t_0) \quad (2)$$

and similarly for $h_n^m(t)$, where t_0 is the middle of the model timespan, that is, 1 March 2024. $\{\dot{g}_n^m, \dot{h}_n^m\}$ are coefficients of the rate of change of the field or Secular Variation (SV). We solve for linear SV up to degree $n = 8$; from $n = 9$ up to $N_{\max} = 40$ the field is considered time-independent.

We adopt the same external field parameterization as used in the CHAOS field model series (Olsen et al., 2006, 2014). This involves two expansions, one representing near magnetospheric sources in the solar magnetic (SM) coordinate system (degree $n = 1$ with time-dependence specified by the ground-based RC index), and a second representing remote magnetospheric sources in the geocentric solar magnetospheric (GSM) coordinates system up to degree 2 but considering only $m = 0$ zonal in GSM terms. Offsets of the RC index are co-estimated in temporal bins of length 5 days, (for degree $n = 1$, order $m = 0$ in SM terms), and in 30-day bins (for degree $n = 1$, order $m = 1$ in SM terms), respectively. Full details of the external field model parameterization can be found in Olsen et al. (2014), our treatment of the associated induced field is described in detail by Finlay et al. (2020).

During field modeling we also co-estimate in-flight alignment Euler angles that rotate the vector magnetic data from the instrument coordinate frame of the VFM to the ASC coordinate frame. We used the "123" Euler angle rotation convention.

Time series of the aberration-corrected Inter Boresight Angle (IBA) between the three cameras of the ASC (Herceg et al., 2017), see Figure S1 in Supporting Information S1, indicate excellent mechanical stability of the optical bench (rms for the 3 IBAs are ≈5 arcsec and <3 arcsec for 20 s running averages). We therefore co-estimate time-independent Euler angles, although we also made test models solving for Euler angles in 10-day bins (see Figure S2 in Supporting Information S1).

MIFM therefore consists of an internal field model up to degree 40 ($40 \times 42 = 1680$ coefficients), an SV model up to degree 8 ($8 \times 10 = 80$ coefficients), an external field model (77 parameters) and one set of Euler angles

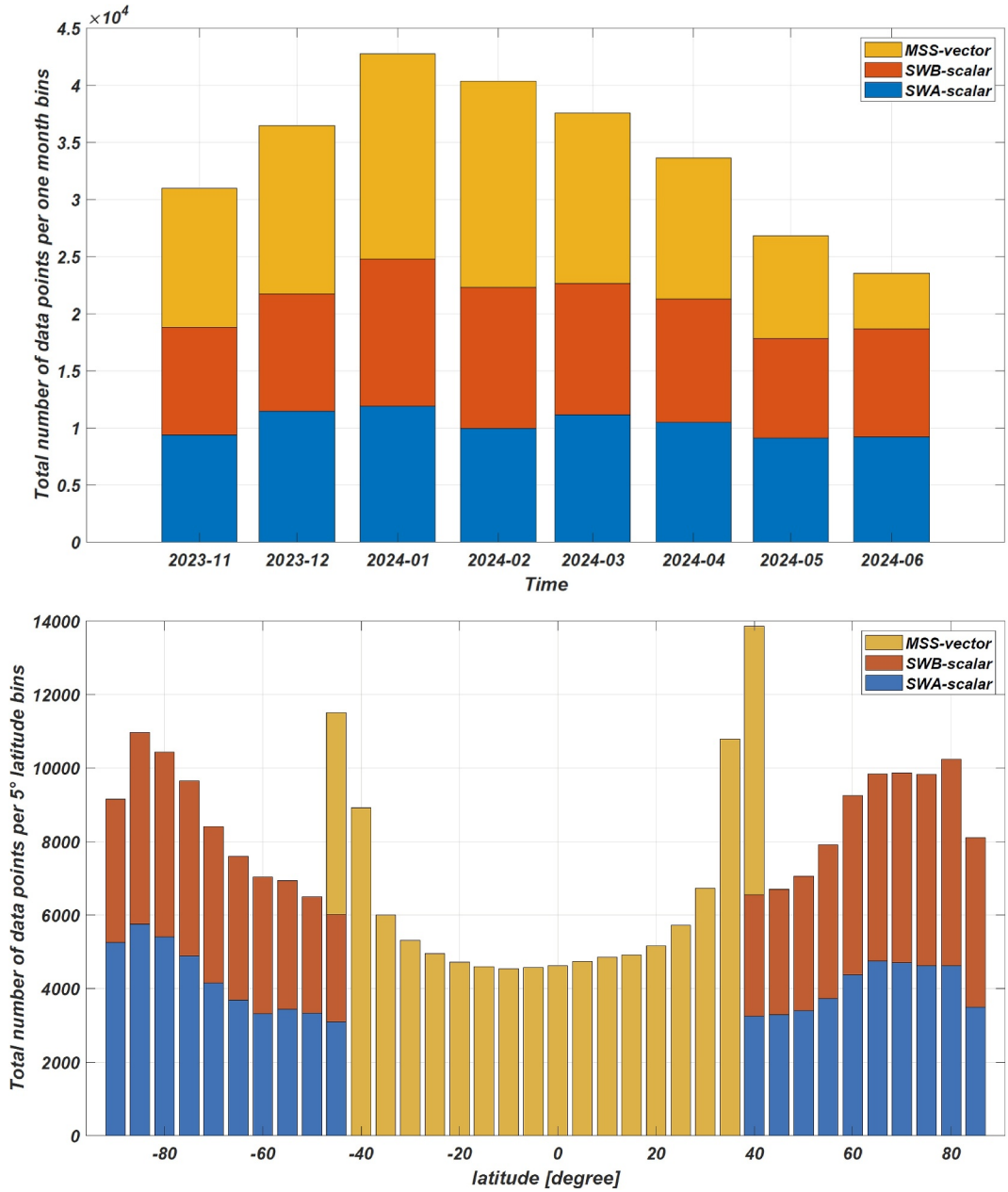

Figure 1. Number of data used in MIFM versus time and geographic latitude in monthly (top) and 5° (bottom) bins, respectively. Number of scalar data are represented as blue (Swarm-A) and red (Swarm-B); Number of vector data are represented as yellow (MSS-1).

(3 parameters). In total, 1,840 model parameters were estimated iteratively by minimizing, using a gradient-descent method, the least-squares loss function

$$\Theta = \mathbf{e}^T \underline{\underline{\mathbf{W}}}\, \mathbf{e} \tag{3}$$

where $\mathbf{e}$ are residuals between the model predictions and the observations and $\underline{\underline{\mathbf{W}}}$ is a diagonal weighting matrix involving robust Huber weights (Constable, 1988; Sabaka et al., 2004) that are iteratively updated, based on residuals from the previous iteration. The weighting matrix included a factor $\sin\theta$ as is appropriate for polar orbiting satellites; we acknowledge that a different latitude-dependent weighting factor should ideally be used for MSS-1 but we have not implemented this in the present study. Starting from a static initial field model for epoch

Table 1
Statistics of the Misfit Between MIFM and MSS-1 and Swarm Satellite Data (Bold, Middle Column)

		Model 1			MIFM			Model_sw		
Satellite	Component	*N*	Mean	Rms	*N*	Mean	Rms	*N*	Mean	Rms
Swarm Alpha	F_{polar}	57,671	−0.79	9.21	**64,942**	**−0.69**	**8.47**	57,671	−0.81	9.20
	$F_{non-polar}$				**17,618**	**−0.09**	**1.86**			
	B_r	77,243	0.07	3.32				77,243	0.07	3.27
	B_θ	77,243	0.09	3.68				77,243	0.23	3.66
	B_ϕ	77,243	−0.07	3.23				77,243	−0.11	3.24
Swarm Bravo	F_{polar}	58,618	−0.21	8.61	**67,040**	**−0.16**	**7.90**	58,618	−0.22	8.58
	$F_{non-polar}$				**18,387**	**0.10**	**1.91**			
	B_r	78,700	0.03	2.32				78,700	−0.02	2.24
	B_θ	78,700	−0.39	3.83				78,700	−0.22	3.77
	B_ϕ	78,700	0.01	3.10				78,700	0.04	3.11
MSS-1	B_r	103,944	0.08 (0.04)	1.92 (1.84)	**103,944**	**0.04 (−0.01)**	**1.96 (1.85)**			
	B_θ	103,944	0.22 (0.16)	3.31 (3.31)	**103,944**	**0.02 (0.01)**	**3.27 (3.27)**			
	B_ϕ	103,944	0.00 (−0.01)	2.83 (2.67)	**103,944**	**0.01 (−0.00)**	**2.76 (2.61)**			

Note. Statistics for similar test models; Model 1 constructed using both MSS-1 and *Swarm* vector data, Model_sw using only *Swarm* data. *N* is number of data, Mean and rms refer to Huber weighted mean and rms misfits in units nT. Numbers in parentheses are misfits to MSS-1 data when in-flight Euler angles are co-estimated in 10 days bins.

2016, MIFM converged (percentage change in all model coefficients less than 0.02%) after 5 iterations. No model regularization was applied.

4. Results

Table 1 presents statistics of the data misfits for the MIFM model (bold, middle column), Model 1 (derived from both MSS-1 and *Swarm* data), and Model_sw derived only from *Swarm* data. The quoted misfits are robust (Huber-weighted) mean and rms misfits. The rms misfits of MIFM to the MSS-1 vector field data lies between 1.96 and 3.27 nT depending on the considered component. This should be compared to the rms misfits of Model_sw to *Swarm* vector data that lie between 2.24 and 3.77 nT (2.00 and 3.39 nT when only data within ±41° latitude are considered). The excellent consistency of MSS-1 and *Swarm* vector data is demonstrated through Model 1 which has misfits to MSS-1 vector data of 1.92 to 3.31 nT and *Swarm* vector data of 2.32 to 3.83 nT. These misfits are dominated by unmodelled geophysical signals; tests show that misfit levels can be further reduced if more sophisticated field models and stringent data selection criteria are employed. We note that the mean residual of B_θ in Model 1 differs between the satellites (+0.09 nT for *Swarm A*, −0.39 nT for *Swarm* B and +0.22 nT for MSS-1), and that similar mean residuals are also found if the vector residuals are converted into a scalar residual. This may indicate an opportunity to make further small improvements in the scalar field calibrations of all the considered satellites.

The MSS-1 in-flight alignment Euler angles co-estimated during the field modeling are found to be very similar (agreeing to within 2 arcsec) regardless of whether only MSS-1 vector data are used (MIFM) or MSS-1 and *Swarm* vector data are used together (Model 1). These in-flight estimated Euler angles, which will be used in the calibration and alignment of the MSS-1 data, differ from pre-flight estimates by around 40 arcsec—a value comparable to that found in previous satellite missions. Test models allowing time-dependence of the Euler angles in 10 days bins (scattering <36 arcsec about the constant MIFM values, see Figure S2 in Supporting Information S1), achieve slightly smaller misfits as they can also absorb variations in unmodelled non-potential fields (see parentheses in Table 1). These results indicate the excellent mechanical stability of the MSS-1 optical platform and the mounting of the instruments.

Detailed comparisons of MIFM to Model 1, Model_sw and the latest model in the CHAOS field model series, CHAOS-7.18 (Finlay et al., 2020) are presented in Figure 2. The top row (left and middle panels) presents Mauersberger-Lowes spectra (Lowes, 1966; Mauersberger, 1956) of the static field and SV, with MIFM shown in

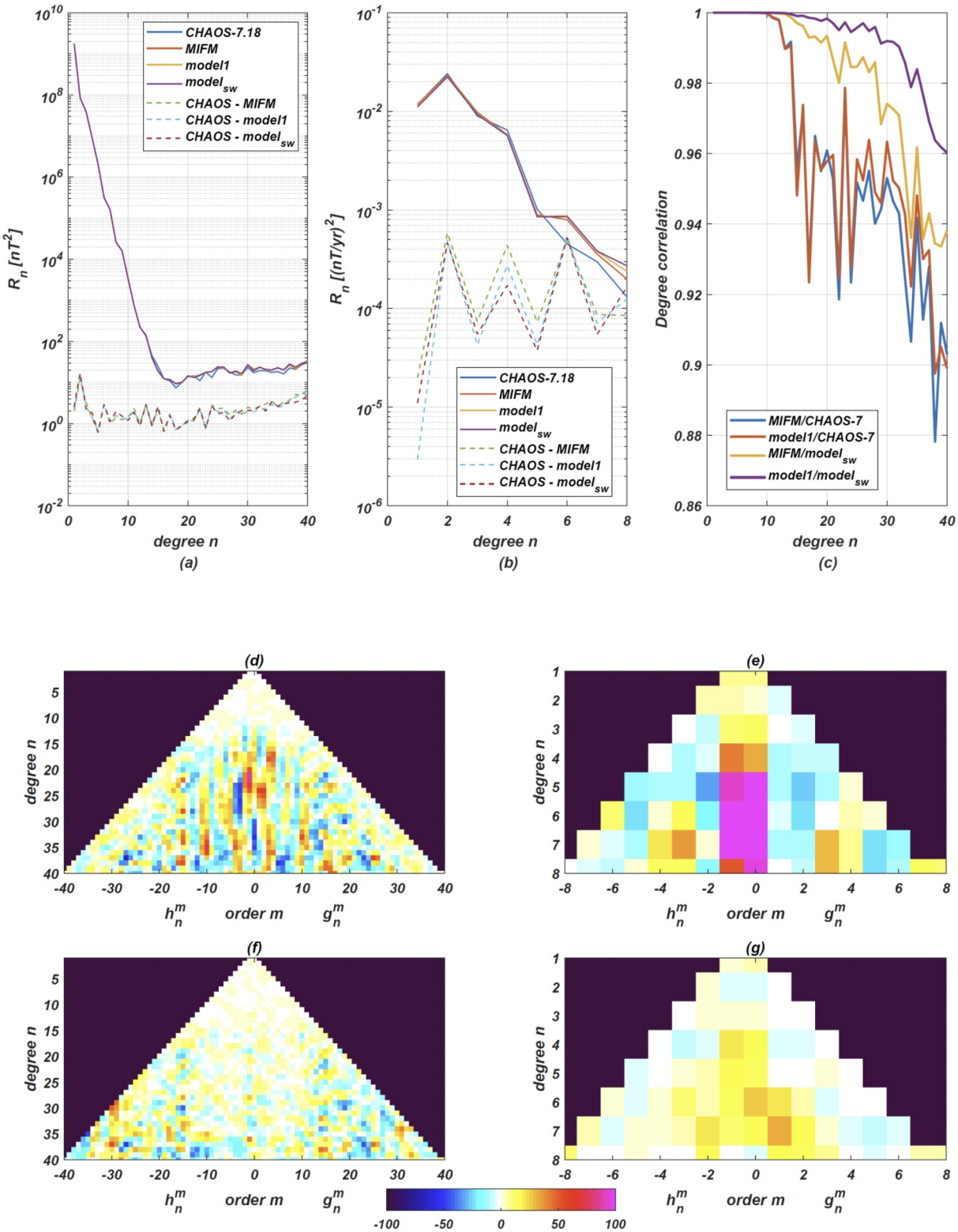

Figure 2. Lowes-Mauersberger spectra (a) of the internal field ($n = 1$–40) and (b) of the linear SV ($n = 1$–8) from various model versions at the Earth's surface. Spectra of models are shown as solid lines, MIFM in red. Spectra of differences between models are shown as dashed lines. (c) Degree correlations of MIFM and Model 1 against CHAOS-7 and Model_sw. Panels (d and e) are coefficient differences (in %), of the static field and SV coefficients respectively, of MIFM compared to CHAOS-7. Panels (f and g) show similar normalized coefficient differences between MIFM and Model_sw.

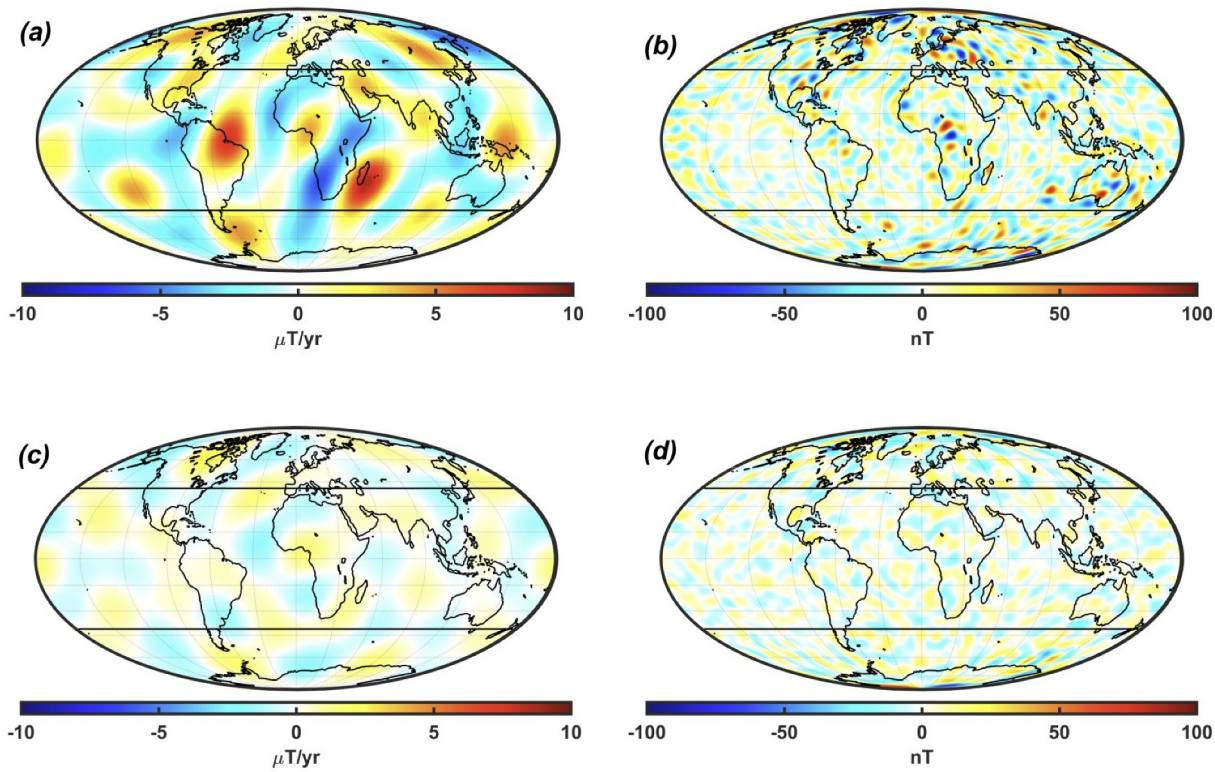

Figure 3. (a) Average rate of change of B_r between November 2023 and June 2024, at the core-mantle boundary, from MIFM up to $n = 8$. Maximum latitudes of MSS-1 data ($\pm 41°$) are marked as black lines. (b) Lithospheric field, B_r at Earth's surface, from MIFM for degree $n = 16 - 40$. (c) Difference in $\dot{B}_r$ between MIFM and CHAOS-7, up to degree 8 but excluding $m = 0, 1$. (d) Difference in B_r at Earth's surface, between MIFM and CHAOS-7 (degree $n = 16 - 40$).

red. All models show very similar spectra for the static fields up to degree 40 and the SV up to degree 5. Above degree 5 the SV spectra for MIFM, Model 1 and Model_sw remain similar up to degree 7 and only diverge slightly at degree 8, with MIFM showing lowest power. CHAOS-7.18 shows lower SV power than the other models from degree 5 to 8, but was derived from a much longer timespan of data, and temporal regularization was used in its construction causing temporal smoothing of the high degree SV (Olsen et al., 2009).

Degree correlations (Sabaka & Olsen, 2006) between MIFM and Model_sw lie above 0.93 for all degrees up to 40 (top right panel of Figure 2), providing further evidence of excellent agreement of MSS-1 and *Swarm* vector field data. The degree correlations of MIFM and Model 1 to CHAOS-7 are slightly lower, but still above 0.9 up to degree 40; differences are expected in this case since the CHAOS-7 lithospheric field above degree 25 is based on the LCS-1 model (Olsen et al., 2017) that was mainly derived using CHAMP vector gradient data from much lower altitudes.

The bottom two rows in Figure 2 present normalized coefficient differences in %, arranged by degree and order (Olsen et al., 2004; Sabaka & Olsen, 2006) for the static field and the SV between MIFM and CHAOS-7 in (d) and (e) and between MIFM and Model_sw in (f) and (g). The corresponding differences between Model_sw and CHAOS-7 are found in Figure S3 of the Supporting Information S1. The largest normalized differences between MIFM and CHAOS-7 occur in the zonal and near zonal coefficients, $m = 0, 1$, in the SV. This is a consequence of limitations in the data coverage at high latitudes over the considered 8 months. On the other hand the near sectorial MF and SV coefficients of MIFM agree very well with CHAOS-7. Turning to normalized coefficient differences between MIFM and Model_sw in Figures 2f and 2g, we find they agree much more closely, confirming that the differences to CHAOS-7 in the near zonal SV coefficients result from the model setup for MIFM and Model_sw, not the MSS-1 data.

Figure 3 presents maps of the radial field SV at the core-mantle boundary up to degree 8 and lithospheric field anomalies (static radial field for degree 14 to 40) at Earth's surface (top row) from MIFM. Also shown are

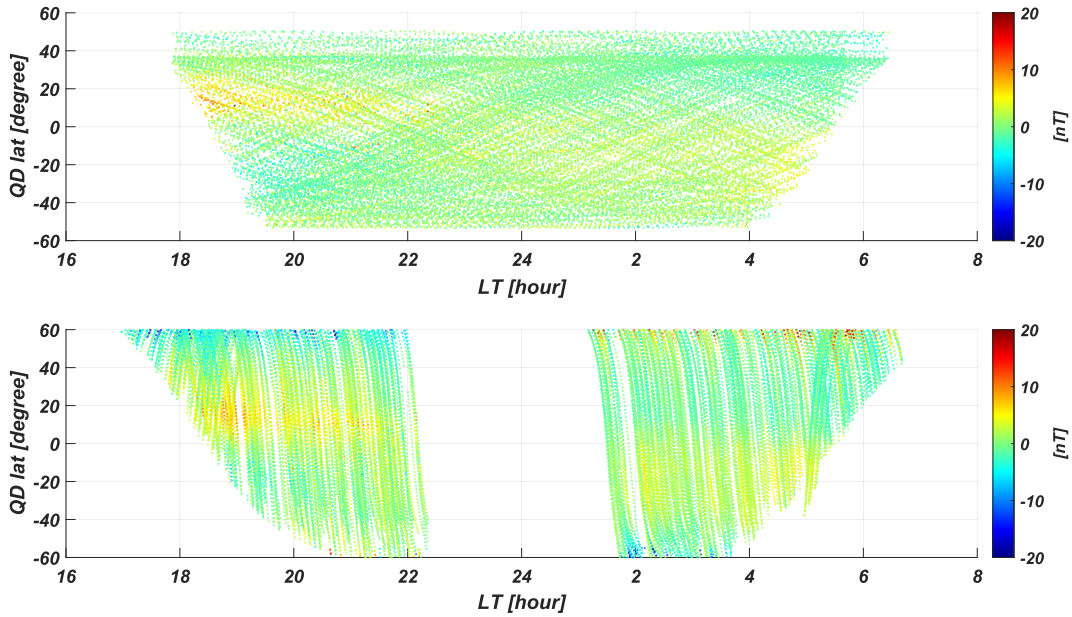

Figure 4. Residuals in the radial component of the magnetic field versus local time (LT) and QD latitude for January and February 2024. Top panel shows residuals between MIFM and MSS-1 data, bottom panel shows residuals between Model_sw and *Swarm* A and B data.

differences between MIFM and CHAOS-7 (bottom row) where the $m = 0, 1$ terms of the SV have been excluded following the discussion above; below latitudes ±40° the rms of these differences are 0.5 μT/yr (for the SV at the CMB) and 5.8 nT (for lithospheric field at Earth's surface) respectively.

Finally we present an example of the impressive local time coverage provided by MSS-1 vector field data. Figure 4 shows radial field residuals (MSS-1 vector data minus MIFM predictions), for two example months, January and February 2024. Also shown for comparison are similar radial field residuals for *Swarm* A and B (*Swarm* data minus predictions of the Model_sw model). See Figures S8 and S9 in Supporting Information S1 for other 2 monthly bins. We recall that MIFM and Model_sw were built using the same geomagnetic quiet-time and dark (Sun at least 10° below horizon) selection criteria. MSS-1 vector data satisfying our field modeling data selection criteria have good coverage of all local times between 20:00 and 04:00. In contrast there are no *Swarm* data covering 22:30 to 01:30. Note that on 1 February 2024 the local time of the ascending node of *Swarm* A was 10:46 and that of *Swarm* B was 02:38. The radial field residuals show coherent signals not captured by our models, most notably a positive anomaly at low QD latitudes in the northern hemisphere between 18:00 and 22:00 likely related to an evening remnant of the Sq current system.

5. Discussion and Conclusion

Eight months of magnetic vector component data from MSS-1 supplemented by field intensity measurements from the *Swarm* A and B satellites at latitudes above ±40°, have been used to construct an initial field model for MSS-1, MIFM, that includes co-estimated in-flight vector field alignment parameters. The resulting MSS-1 vector field components show Huber-weighted rms residuals to MIFM of (1.96, 3.27, 2.76) nT respectively for (B_r, B_θ, B_ϕ) which compares favorably with the rms misfits of (2.00, 3.39, 3.17) nT found for *Swarm* vector data below 41° latitude compared to a similar *Swarm*-only field model. MSS-1 and *Swarm* vector data can also be fit simultaneously, with only very small increases in misfit. These findings indicate a successful calibration and alignment of MSS-1 vector data resulting in stable and robust vector magnetic data with absolute accuracy, suitable for high quality geomagnetic field modeling.

MIFM agrees well with the latest CHAOS-7 field model up to spherical harmonic degree 40 in the static field and up to degree 8 in the SV, except for near zonal terms above degree 5 in the SV, that are affected by limitations in dark data coverage provided by *Swarm* at high latitudes over the considered 8 months. Even better agreement is

found between MIFM and a similarly parameterized field model constructed using only data from the *Swarm* A and B satellites covering the same 8 months.

Maps of the lithospheric field from MIFM show the expected strong continental anomalies, for example, the Bangui anomaly in West central Africa, in eastern North America and in Australia. The core-mantle boundary radial field SV from MIFM is, as expected, dominated by high amplitude localized SV foci at mid-to-low latitudes, for example, below Southern Africa and eastern South America. MIFM was able to retrieve these core field SV foci despite being based on only 8 months of data and employing no model regularization. MSS-1 vector data can therefore be used to study both lithospheric magnetization features and core dynamics, in particular rapidly evolving low latitude field features (Finlay et al., 2023; Gillet et al., 2022; Jackson, 2003). Improved field resolution is expected as longer timespans of MSS-1 data become available, as it descends to lower altitudes, and once use is made of gradients along its unusual low inclination orbit.

The improved local time coverage provided by high quality MSS-1 vector data opens the door to new approaches to studying the geomagnetic field, going beyond the traditional field modeling techniques used here. Large-scale ionospheric and magnetospheric fields at mid and low latitudes can now be studied from space across all local times on timescales down to 2 months. Efforts are now needed to better exploit the combination of MSS-1 and *Swarm* data, making the most of their different orbital characteristics, this is a direction which we plan to pursue in our future work. MSS-1 represents an important step toward a more complete global geomagnetic observing system, but there are further exciting advances on the horizon with the MSS-2 (Jiang et al., 2023; K. Zhang, 2023) and NanoMagSat (Hulot et al., 2018) missions that are planned for launch as we move toward the next solar minimum.

Data Availability Statement

The MSS-1 data used in the study are available at https://mss.must.edu.mo/data.html.

The Swarm data are available at https://earth.esa.int/eogateway/missions/swarm/data.

The CHAOS-7 model and its updates are available at http://www.spacecenter.dk/files/magnetic-models/CHAOS-7/.

Acknowledgments
Thanks to the China National Space Administration and the Macau Foundation for their support. We wish to thank all personnel at DFH, DTU, IWF, NSSC, and MUST for their contributions to satellite launch and data processing. Y.J. is supported by the National Natural Science Foundation of China (12250012, 12250014, 42250101, 42250102, 42250103). The work of C.C.F., N.O., and L.T.-C. has been carried out as part of *Swarm* DISC activities, funded by ESA contract no. 4000109587.

References

Brauer, P., Merayo, J., Risbo, T., & Primdahl, F. (2001). Magnetic calibration of vector magnetometers: Linearity, thermal effects and stability, ESA SP-490. In F. Primdahl, & A. Balogh (Eds.), *Ground and in-flight space magnetometer calibration techniques*.

Constable, C. G. (1988). Parameter estimation in non-Gaussian noise. *Geophysical Journal International*, *94*(1), 131–142. https://doi.org/10.1111/j.1365-246x.1988.tb03433.x

Finlay, C. C., Gillet, N., Aubert, J., Livermore, P. W., & Jault, D. (2023). Gyres, jets and waves in the Earth's core. *Nature Reviews Earth & Environment*, *4*(6), 377–392. https://doi.org/10.1038/s43017-023-00425-w

Finlay, C. C., Kloss, C., Olsen, N., Hammer, M. D., Tøffner-Clausen, L., Grayver, A., & Kuvshinov, A. (2020). The CHAOS-7 geomagnetic field model and observed changes in the South Atlantic Anomaly. *Earth Planets and Space*, *72*(1), 156. https://doi.org/10.1186/s40623-020-01252-9

Friis-Christensen, E., Lühr, H., & Hulot, G. (2006). Swarm: A constellation to study the Earth's magnetic field. *Earth Planets and Space*, *58*(4), 351–358. https://doi.org/10.1186/bf03351933

Gillet, N., Gerick, F., Jault, D., Schwaiger, T., Aubert, J., & Istas, M. (2022). Satellite magnetic data reveal interannual waves in Earth's core. *Proceedings of the National Academy of Sciences of the United States of America*, *119*(13), e2115258119. https://doi.org/10.1073/pnas.211525811

Herceg, M., Jørgensen, P. S., & Jørgensen, J. L. (2017). Stellar aberration correction and thermo-elastic compensation of Swarm μASC attitude observations. *Geophysical Journal International*, *211*(2), 1104–1107. https://doi.org/10.1093/gji/ggx285

Hulot, G., Léger, J.-M., Vigneron, P., Jager, T., Bertrand, F., Coïsson, P., et al. (2018). Nanosatellite high-precision magnetic missions enabled by advances in a stand-alone scalar/vector absolute magnetometer. In *IGARSS 2018—2018 IEEE international geoscience and remote sensing symposium* (pp. 6320–6323).

Jackson, A. (2003). Intense equatorial flux spots on the surface of Earth's core. *Nature*, *464*, 760–763.

Jiang, Y., Olsen, N., Ou, J., & Yan, Q. (2023). Simulation for MSS-2 low-perigee elliptical orbit satellites: An example of lithospheric magnetic field modelling. *Earth and Planetary Physics*, *7*(1), 151–160. https://doi.org/10.26464/epp2023021

Jørgensen, J., Denver, T., Betto, M., & Jørgensen, P. (2003). Micro ASC, a miniature star tracker. In H.-P. Röser, R. Sandau, & V. Arnoldo (Eds.), *Small satellites for Earth observation, 4th international symposium of the international academy of astronautics* (pp. 157–162).

Lowes, F. J. (1966). Mean-square values on sphere of spherical harmonic vector fields. *Journal of Geophysical Research*, *71*(8), 2179. https://doi.org/10.1029/jz071i008p02179

Mauersberger, P. (1956). Das Mittel der Energiedichte des geomagnetischen Hauptfeldes an der Erdoberfläche und seine säkulare Änderung. *Gerlands Beitrage zur Geophysik*, *65*, 207–215.

Merayo, J. M. G., Brauer, P., Primdahl, F., Petersen, J. R., & Nielsen, O. V. (2000). Scalar calibration of vector magnetometers. *Measurement Science and Technology*, *11*(2), 120–132. https://doi.org/10.1088/0957-0233/11/2/304

Olsen, N., Friis-Christensen, E., Hulot, G., Korte, M., Kuvshinov, A., Lesur, V., et al. (2004). Swarm end-to-end mission performance simulator study. *DSRI Report*, *1*, 1–190.

Olsen, N., Lühr, H., Sabaka, T., Michaelis, I., Rauberg, J., & Tøffner-Clausen, L. (2014). The CHAOS-4 geomagnetic field model. *Geophysical Journal International*, *1997*, 815–827.

Olsen, N., Lühr, H., Sabaka, T. J., Mandea, M., Rother, M., Tøffner-Clausen, L., & Choi, S. (2006). CHAOS—A model of the Earth's magnetic field derived from CHAMP, Ørsted, and SAC-C magnetic satellite data. *Geophysical Journal International*, *166*(1), 67–75. https://doi.org/10.1111/j.1365-246x.2006.02959.x

Olsen, N., Mandea, M., Sabaka, T. J., & Tøffner-Clausen, L. (2009). CHAOS-2—-a geomagnetic field model derived from one decade of continuous satellite data. *Geophysical Journal International*, *179*(3), 1477–1487. https://doi.org/10.1111/j.1365-246X.2009.04386.x

Olsen, N., Ravat, D., Finlay, C. C., & Kother, L. K. (2017). LCS-1: A high-resolution global model of the lithospheric magnetic field derived from CHAMP and Swarm satellite observations. *Geophysical Journal International*, *211*(3), 1461–1477. https://doi.org/10.1093/gji/ggx381

Richmond, A. D. (1995). Ionospheric electrodynamics using magnetic apex coordinates. *Journal of Geomagnetism and Geoelectricity*, *47*(2), 191–212. https://doi.org/10.5636/jgg.47.191

Sabaka, T. J., & Olsen, N. (2006). Enhancing comprehensive inversions using the *Swarm* constellation. *Earth Planets and Space*, *58*(4), 371–395. https://doi.org/10.1186/BF03351935

Sabaka, T. J., Olsen, N., & Purucker, M. E. (2004). Extending comprehensive models of the Earth's magnetic field with Ørsted and CHAMP data. *Geophysical Journal International*, *159*(2), 521–547. https://doi.org/10.1111/j.1365-246x.2004.02421.x

Shi, Y., Li, L., Chen, J., Zuo, F., Zhang, X., Mei, Z., et al. (2023). Design of the solar X-ray detector for the Macau Science Satellite-1B. *Earth and Planetary Physics*, *7*(1), 125–130. https://doi.org/10.26464/epp2023018

Winch, D. E., Ivers, D. J., Turner, J. P. R., & Stening, R. J. (2005). Geomagnetism and Schmidt quasi-normalization. *Geophysical Journal International*, *160*(2), 487–504. https://doi.org/10.1111/j.1365-246x.2004.02472.x

Zhang, H., Yu, C., Suo, L., Luo, W., Yuan, D., & Ou, J. (2023). Thermal stability analysis of a satellite-borne optical bench based on quasi-kinematic support. *Earth and Planetary Physics*, *7*(1), 119–124. https://doi.org/10.26464/epp2023020

Zhang, K. (2023). A novel geomagnetic satellite constellation: Science and applications. *Earth and Planetary Physics*, *7*(1), 4–21. https://doi.org/10.26464/epp2023019